Non-Newtonian Topological Mechanical Metamaterials Using Feedback Control

Lea Sirota,[1,2,*] Roni Ilan,[1] Yair Shokef,[2,3,4,5] and Yoav Lahini[1,5]
[1]Raymond and Beverly Sackler School of Physics and Astronomy, Tel-Aviv University, Tel Aviv 69978, Israel
[2]School of Mechanical Engineering, Tel Aviv University, Tel Aviv 69978, Israel
[3]Sackler Center for Computational Molecular and Materials Science, Tel Aviv University, Tel Aviv 69978, Israel
[4]Center for Nonlinear Studies, Los Alamos National Laboratory, Los Alamos, New Mexico 87545, USA
[5]The Center for Physics and Chemistry of Living Systems, Tel Aviv University, Tel Aviv 69978, Israel

(Received 5 March 2020; accepted 30 October 2020; published 18 December 2020)

We introduce a method to design topological mechanical metamaterials that are not constrained by Newtonian dynamics. The unit cells in a mechanical lattice are subjected to active feedback forces that are processed through autonomous controllers preprogrammed to generate the desired local response in real time. As an example, we focus on the quantum Haldane model, which is a two-band system with nonreciprocal coupling terms, the implementation of which in mechanical systems requires violating Newton's third law. We demonstrate that the required topological phase characterized by chiral edge modes can be achieved in an analogous mechanical system only with closed-loop control. We then show that our approach enables us to realize, a modified version of the Haldane model in a mechanical metamaterial. Here, the complex-valued couplings are polarized in a way that modes on opposite edges of a lattice propagate in the same direction, and are balanced by counterpropagating bulk modes. The proposed method is general and flexible, and could be used to realize arbitrary lattice parameters, such as nonlocal or nonlinear couplings, time-dependent potentials, non-Hermitian dynamics, and more, on a single platform.

DOI: 10.1103/PhysRevLett.125.256802

The discovery of topologically protected wave phenomena in quantum physics [1–4] with their exceptional immunity to backscattering has recently inspired the search for realizations in classical systems, substituting the electronic band structure with acoustic [5–8] or photonic [9–13] dispersion relations. These classical analogs are not merely a way to mimic well-known effects, but also a way to push the study of topological physics to new regimes [14–22]. However, systems governed by Newtonian dynamics, such as mechanical structures supporting acoustic or elastic waves, usually do not naturally exhibit topological properties [23]. This insight is driving the current surge of activity aimed at designing topological mechanical metamaterials [24–32].

The particular quantum effect considered for the classical realization dictates the metamaterial design. As classical-mechanical systems are constrained by Newtonian laws of motion, the range of known topological phenomena that can be observed is limited. The quantum spin Hall effect [3,4] or the quantum valley Hall effect [33], for which the spin-orbit coupling is obtained through breaking spatial symmetry in a lattice, comply with Newtonian dynamics, and can be implemented with purely passive components. Indeed, the vast majority of reports on mechanical topological metamaterials implement these effects, e.g., by designing the spacing of steel bars [7] or bottlelike Helmholtz resonators [8] in an acoustic waveguide, the spacing of resonators on a plate [29], the spring constants in a mass-spring lattice [30], or a pendula array with intricate couplings [24], to name a few.

Some quantum phases, however, defy such a straightforward classical analog. For example, creating an acoustic analog of the quantum Hall effect, which requires breaking time reversal symmetry (TRS) (i.e., a Chern insulator), is considerably more involved, as passive design becomes insufficient. Consequently, there have only been a few reports of TRS breaking in mechanical or acoustic systems; for fixed parameters and excitation frequency, a Chern insulator was emulated in a lattice of gyroscopes [25,26] and in a system of circulating fluids [5,34]. These realizations require auxiliary in-plane degrees of freedom (d.o.f.), i.e., actual physical in-plane rotation of masses or fluids. Another method based on Floquet acoustic crystals employed temporal modulation of the acoustic parameters or the frequency [15–17]. These methods increase the complexity of the physical realization compared to the desired model—for example they necessarily result in additional dispersion bands.

It would be advantageous to break TRS with time-invariant parameters in a two-band metamaterial with out-of-plane d.o.f. alone, i.e., 1 d.o.f. per mass. This is because it will enable reproduction of quantum effects that are associated with two-band systems [2,35–39]. In addition, it appears more feasible to realize such systems experimentally, as out-of-plane d.o.f. imply a scalar field, such as acoustic pressure or flexural waves. However, when

only out-of-plane d.o.f. (and time invariant parameters) are allowed, breaking TRS in acoustic or mechanical metamaterials requires lattice couplings that are inconsistent with the governing physical laws, including complex-valued directional, or nonreciprocal couplings, as discussed below.

In this Letter, we present a general method of realizing mechanical metamaterials that are not constrained by Newtonian laws of motion. At the heart of our method is the application of active forces to the masses in the out-of-plane direction, in real time and autonomously, according to a predefined, programmable feedback control scheme. To be concrete, we focus on a particular example and show how it is possible to break TRS using only out-of-plane d.o.f., with a single d.o.f. per site in a discrete mechanical lattice.

Employing active control in the design of metamaterials has recently attracted considerable interest [18–22,40–46]. In our system, an autonomous preprogrammed controller in each unit cell receives measurements of displacements and velocities of masses in neighboring lattice sites, processes them, and feeds back to the control forces. The control operation therefore determines, in real time, the dynamic response of the masses. Since the particular couplings are solely defined by the algorithm that we program into the controller, the feedback-based metamaterial is able to sustain any couplings (within hardware limitations), including those that are otherwise physically not achievable, such as directional or nonreciprocal couplings. Furthermore, a single system is not limited to emulate a particular quantum effect, but can be programmed to any other functionality.

We demonstrate our feedback-based design method by implementing, analytically and numerically, a classical-mechanical analog of the quantum Haldane model [2], and the modified quantum Haldane model [35–39]. Both systems require non-Newtonian physics, which can be achieved only by the embedded feedback control mechanism. Below we present a detailed derivation of the controller that implements the Haldane model. For the modified Haldane model, we show only the resulting dynamical simulations, with the details given in the Supplemental Material [47]. To further demonstrate the versatility of our method, in the Supplemental Material [47] we also reprogram the embedded controller to realize a multipole pseudospin topological insulator on the same platform.

The Haldane model showed that the quantum Hall effect can be obtained without an external magnetic field, but rather by breaking TRS. It is defined on a honeycomb lattice spanned by $\{\mathbf{a}_1, \mathbf{a}_2\}$, which consists of two interlacing triangular sublattices exhibiting two sites per unit cell A and B, as illustrated in Fig. 1(a). We denote the lattice constant by a. In our classical-mechanical analog, the circles are identical dimensionless masses $m_0 = 1$ that can vibrate only along the vertical axis $\mathbf{a}_3$. The gray bars indicate nearest-neighbor couplings, which are equivalent

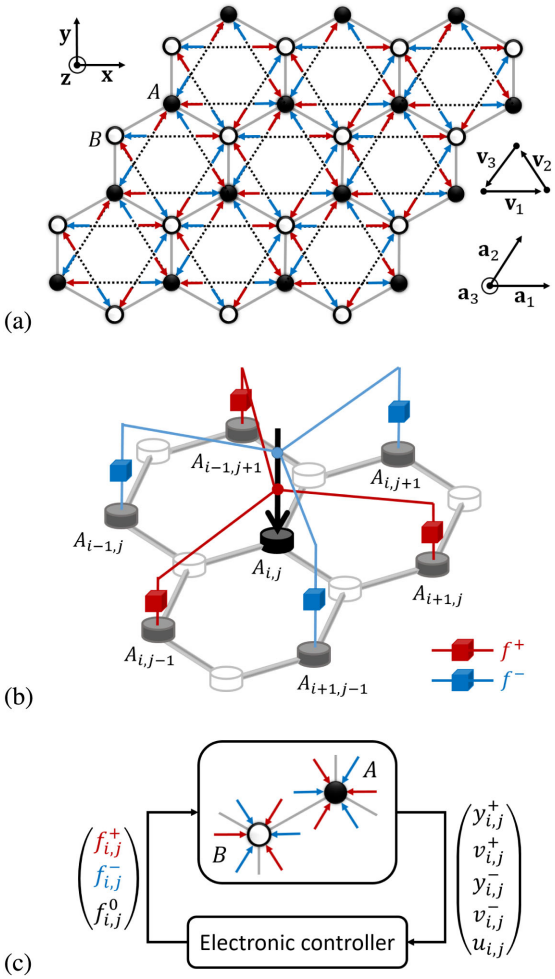

FIG. 1. Feedback control scheme for generating the Haldane model in a mechanical metamaterial. (a) A honeycomb lattice in the $\{\mathbf{a}_1, \mathbf{a}_2\}$ space comprising identical masses (black and white circles) connected to nearest neighbors by Hookean springs (gray bars). The masses can move in the $\mathbf{a}_3$ (out-of-plane) direction only, implying a single d.o.f. per site. The red and blue arrows indicate out-of-plane displacement and velocity measurements of the next-nearest neighbors (in $\{\mathbf{v}_1, \mathbf{v}_2, \mathbf{v}_3\}$ directions). Dashed lines indicate the Haldane model bonds that are created in real time when control is turned on. (b) The measurement scheme detailed for the A site in the $\{i, j\}$ unit cell. The black arrow indicates the total control force $f^A = f^+ + f^- + f^0$. Red and blue arrows distinguish between measurements that are fed to controller gains $t_2 e^{+i\phi}$ and $t_2 e^{-i\phi}$ (red and blue cubes), applied through the f^+ and f^- components, respectively. (c) Feedback control scheme of the entire $\{i, j\}$ unit cell, including all the measured signals.

to Hookean springs of stiffness $t_1 > 0$ connecting the masses. When only the t_1 springs exist, the lattice is analogous to graphene.

The quantum Haldane model assumes additional next-nearest-neighbor bonds of a complex strength $t_2 e^{\pm i\phi}$ in the directions $\mathbf{v}_1$, $\mathbf{v}_2$, $\mathbf{v}_3$ indicated by the dashed black lines in Fig. 1(a). In a mechanical context, such a bond represents a

nonreciprocal coupling $t_2 e^{+i\phi}$ (red arrow) toward one mass and $t_2 e^{-i\phi}$ (blue arrow) toward the other connected mass, which violates Newton's third law and is therefore nonphysical. These couplings cannot be implemented with passive devices such as springs, lever arms, etc., or with auxiliary active devices like gyroscopes that rely on in-plane d.o.f. We realize these couplings using active closed-loop control. Contrary to usual expectations, the complex values of the forces are physical in the time-harmonic regime because they are related to velocities rather than to displacements. The full form of the Haldane model is captured by the Bloch Hamiltonian $H(\mathbf{k}) = \sum_{l=0}^{3} \mathcal{H}_l(\mathbf{k})\sigma_l$, where $\mathbf{k}$ is the wave vector, σ_l are the Pauli matrices, and

$$\begin{aligned}
\mathcal{H}_0 &= \beta + 2t_2 \cos\phi \sum_{m=1}^{3} \cos(\mathbf{k}\cdot\mathbf{v}_m),\\
\mathcal{H}_1 &= -t_1\big(1 + \cos(\mathbf{k}\cdot\mathbf{a}_1) + \cos(\mathbf{k}\cdot\mathbf{a}_2)\big),\\
\mathcal{H}_2 &= t_1\big(\sin(\mathbf{k}\cdot\mathbf{a}_1) + \sin(\mathbf{k}\cdot\mathbf{a}_2)\big),\\
\mathcal{H}_3 &= M - 2t_2 \sin\phi \sum_{m=1}^{3} \sin(\mathbf{k}\cdot\mathbf{v}_m).
\end{aligned} \tag{1}$$

In a quantum system, $\beta = 0$. In the classical-mechanical analog of graphene $\beta = 3t_1$, indicating the restoring t_1 force from the three nearest-neighbor springs and it is not related to Haldane's next-nearest-neighbor bonds. The constant M accounts for a possible spatial inversion symmetry breaking, in addition to the TRS breaking provided by the t_2 bonds.

The goal of our embedded control system is to create a classical-mechanical metamaterial, whose dynamics in lattice momentum space $\mathbf{k}$ is given by

$$\omega^2 \mathbf{p}(\mathbf{k}) = H(\mathbf{k})\mathbf{p}(\mathbf{k}). \tag{2}$$

Here, $H(\mathbf{k})$ is the Bloch Hamiltonian of the Haldane model, and $\mathbf{p}(\mathbf{k})$ is the complex amplitude vector of the A and B sites in momentum space. Our starting point is the graphenelike lattice (t_1 springs only), in which we denote the d.o.f. of each $\{i,j\}$ unit cell by $\mathbf{u}_{i,j}(t) = [\,u^A_{i,j}(t), u^B_{i,j}(t)\,]^T$. The time domain unit cell dynamics, including external mechanical control forces $f^A_{i,j}, f^B_{i,j}$ that are applied to the masses in the a_3 direction, reads

$$\begin{aligned}
\ddot{u}^A_{i,j} &= -3t_1 u^A_{i,j} + t_1(u^B_{i,j} + u^B_{i+1,j} + u^B_{i,j+1}) + f^A_{i,j},\\
\ddot{u}^B_{i,j} &= -3t_1 u^B_{i,j} + t_1(u^A_{i,j} + u^A_{i-1,j} + u^A_{i,j-1}) + f^B_{i,j}.
\end{aligned} \tag{3}$$

The control forces are decomposed into $f^A_{i,j} = f^{A+}_{i,j} + f^{A-}_{i,j} + f^{A0}_{i,j}$ and $f^B_{i,j} = f^{B+}_{i,j} + f^{B-}_{i,j} + f^{B0}_{i,j}$. The f^+ and f^- components are responsible for generating the $t_2 e^{+i\phi}$ and the $t_2 e^{-i\phi}$ couplings, respectively, and f^0 is responsible for generating M. As depicted in Fig. 1(b), e.g., for the A site, the f^{A+} and f^{A-} components receive measured signals of displacements and velocities of the $u^A_{i+1,j}, u^A_{i-1,j+1}, u^A_{i,j-1}$ and $u^A_{i-1,j}, u^A_{i+1,j-1}, u^A_{i,j+1}$ d.o.f., as indicated by the red and blue arrows, respectively. These arrows are also shown on the multicell lattice segment in Fig. 1(a). The f^{A0} component is not depicted. The measurements are processed in real time by corresponding controllers indicated by red and blue cubes. The control action is illustrated in Fig. 1(c) for the $\{i,j\}$ unit cell. For each site A and B (the superscripts are omitted in the following), the control forces are related to the measured signals as

$$(f^+_{i,j} \quad f^-_{i,j} \quad f^0_{i,j})^T = C(\,y^+_{i,j} \quad v^+_{i,j} \quad y^-_{i,j} \quad v^-_{i,j} \quad u_{i,j}\,)^T, \tag{4}$$

where, for the A site,

$$\begin{aligned}
y^\pm_{i,j} &= u_{i\pm1,j} + u_{i\mp1,j\pm1} + u_{i,j\mp1},\\
v^\pm_{i,j} &= \dot{u}_{i\pm1,j} + \dot{u}_{i\mp1,j\pm1} + \dot{u}_{i,j\mp1}.
\end{aligned} \tag{5}$$

For the B site, the definitions of $y^+(v^+)$ and $y^-(v^-)$ in Eq. (5) are swapped. The control matrix C at each $\{i,j\}$ unit cell, for both A and B sites, is given by

$$C = \begin{pmatrix} t_2\cos\phi & \frac{t_2}{\omega}\sin\phi & 0 & 0 & 0\\ 0 & 0 & t_2\cos\phi & -\frac{t_2}{\omega}\sin\phi & 0\\ 0 & 0 & 0 & 0 & \pm M \end{pmatrix}. \tag{6}$$

The sign of M in Eq. (6) is positive (negative) for the A (B) sites. Since in the frequency domain, the velocity v is related to the displacement u as $v = i\omega u$, the controller gains that generate the velocity couplings are normalized by the frequency of the source signal, which is a fixed scalar in a given working regime. This normalization guarantees the frequency independence of the complex-valued nonreciprocal next-nearest-neighbor couplings required by the Haldane model Hamiltonian (1), which are created by the control forces in real time. The resulting closed-loop system is dynamically stable, and the control forces do not exceed the source force amplitude.

A two-band system implies a scalar dynamical field, which significantly reduces the complexity of experimental realization compared to systems with higher number of bands. One possibility is implementation in an actual discrete mechanical system. The out-of-plane displacement may then be achieved by constraining weights, horizontally connected to nearest neighbors by prestressed harmonic springs, to move on vertical shafts through linear bearings. The spring constant needs to be tuned carefully to balance between friction reduction and dominance over gravity. An alternative implementation is by an acoustic pressure field created in a two-dimensional waveguide by an array of loudspeakers. In both scenarios, the feedback control system in Eqs. (3)–(6) is realized by an autonomous

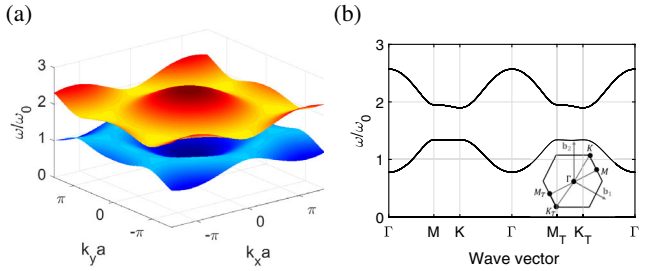

FIG. 2. Infinite lattice dispersion relations of the Haldane model mechanical analog. Dispersion diagram with parameters $\{t_2 = 0.2t_1, \phi = \pi/3, M = 0\}$ is plotted over the entire Brillouin zone (a) and through the high symmetry points (b).

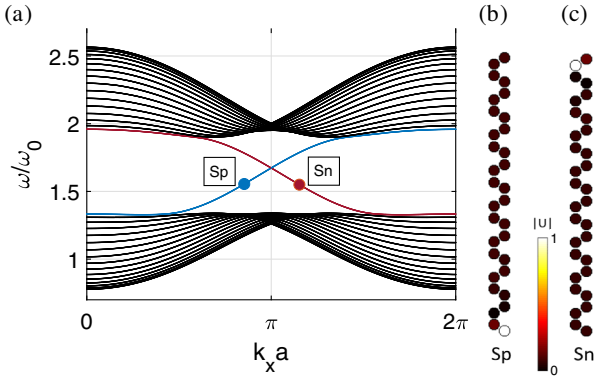

FIG. 3. Edge modes of the mechanical Haldane model. (a) Dispersion diagram of a lattice infinite in the **x** direction and of eight honeycomb cells in the **y** direction. Black lines indicate bulk states. The red (blue) line indicates top (bottom) edge state with negative (positive) group velocity. (b),(c) Corresponding eigenmodes of top and bottom edge states.

microcontroller that processes the measurements at corresponding next-nearest-neighbor locations.

Next we demonstrate that the mechanical system (2) governed by the classical analog of the Haldane model Hamiltonian (1), which we created with the control system (4)–(6), reproduces all the known dynamic properties of the quantum Haldane model. This is not obvious, since the complex-valued couplings are retained only upon reaching the time-harmonic regime. The first property that we analyze is the band structure, here the acoustic dispersion, of an infinite lattice. Since Eq. (2) represents a classical-mechanical system, the eigenvalues are squared frequencies. The frequencies are kept real and positive due to the constant shift of the dispersion curves by the addition of $\beta = 3t_1$ to the σ_0 term in Eq. (1). Since this addition does not change the eigenvectors, the metamaterial preserves the topological properties of the original quantum Haldane model. We consider, for example, $\{\phi = \pi/3, M = 0, t_2 = 0.2t_1\}$, which falls within the nontrivial topological regime of Chern number $n = +1$, according to the phase diagram of the quantum Haldane model [2]. The corresponding band structure is depicted in Fig. 2. The frequency scale is normalized by $\omega_0 = \sqrt{t_1/m_0}$. See the Supplemental Material [47] for a different set of parameters and for the actual parameter scale. Similar to the quantum system, the band structure is not symmetric between the $\Gamma - M - K - \Gamma$ and the $\Gamma - M_T - K_T - \Gamma$ trajectories.

Next we verify the reproduction of the quantum edge mode dispersion. Now our lattice is infinite in **x** but finite in the **y** direction. The dispersion diagram of an eight honeycomb cells strip is plotted in Fig. 3(a). As expected for the Haldane model, a state emerges inside the bulk band gap, corresponding to top edge propagation with negative group velocity (S_n point) and to bottom edge propagation with positive group velocity (S_p point). The eigenmodes associated with these counterpropagating chiral edge states are depicted in Figs. 3(b) and 3(c). The wave localization on the lattice edge is guaranteed by the topological property of the band structure.

Recently, a modified version of the Haldane model was proposed [35–38]. Here, both top and bottom edge modes propagate in the same direction, compensated by bulk modes that propagate in the opposite direction. Such antichiral edge states can exist in two-dimensional lattices if the bulk band structure is gapless, as the number of left and right moving modes in a finite system must be the same. A significant suppression of backscattering is provided for the edge modes due to their spatial separation from the bulk modes, whereas the bulk modes diffuse across the lattice width. To obtain the modified Haldane model, one needs to flip the direction of the complex-valued next-nearest-neighbor couplings of one of the unit cell sites, e.g., of the B site in Fig. 1(a). The resulting mechanical analog is a two-band non-Newtonian system, similar to the original Haldane model, and can be realized in mechanical systems only with a feedback mechanism. The finite lattice band structure and the corresponding controller are given in the Supplemental Material [47].

We now demonstrate that our metamaterial supports unidirectional edge wave propagation, as expected for both the original and the modified Haldane models. We perform two dynamical simulations of a finite size metamaterial (20×40 honeycomb net), which is operated in a real-time feedback loop; see Fig. 4. Fixed boundary conditions along all edges are assumed, and the actuation frequency is set to $\omega = 1.55\omega_0$. The system is excited by a time-harmonic force $F(t) = F_0 e^{i\omega t}$ in the $\mathbf{a}_3$ direction at the middle of the top and bottom edges, as indicated by the blue arrows in the figure. Closed-loop time responses of the masses out-of-plane displacements $u_{i,j}(t)$ (normalized by F_0) are shown at two time instances, $T_1 < T_2$. At these times the control transients converged, and the system reached its dynamical steady state.

Figures 4(a) and 4(b) correspond to control program 1, creating the Haldane model (1), according to Eqs. (2)–(6) with $\{t_2 = 0.2t_1, \phi = \pi/3, M = 0\}$. Here the actuation frequency lies inside the bulk band gap. One clearly sees

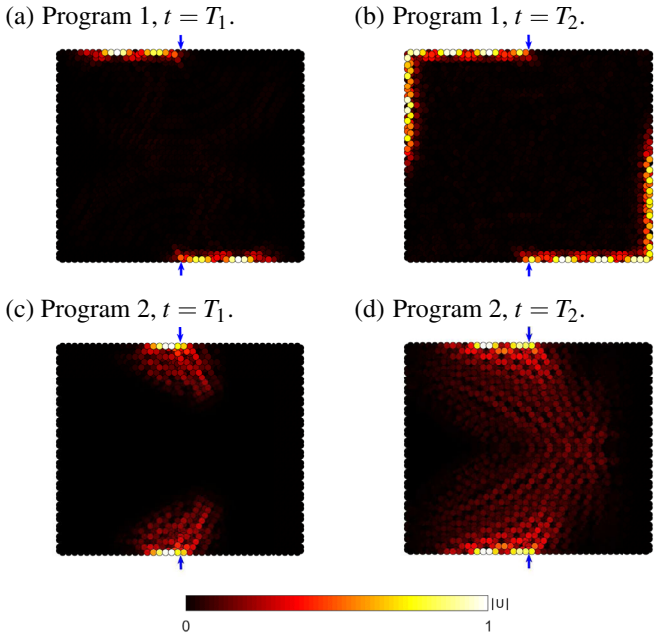

FIG. 4. Dynamical simulation of the feedback-based mechanical metamaterial. A force $F(t) = F_0 e^{i\omega t}$ indicated by the blue arrows is applied to a 20×40 honeycomb lattice in the $\mathbf{a}_3$ direction. The displacement responses of the masses in $\mathbf{a}_3$ are depicted at time instances $T_1 < T_2$ (left and right columns). (a), (b) Control program 1 realizing the Haldane model. (c),(d) Control program 2 realizing the modified Haldane model.

that at the top (bottom) edge the wave propagates to the left (right) corresponding to the S_n (S_p) point in Fig. 3(a). Because of topological protection, the wave circumvents the sharp lattice corners without any backscattering. Figures 4(c) and 4(d) correspond to control program 2, creating the modified Haldane model with $\{t_2 = 0.1t_1, \phi = \pi/3, M = 0\}$. As expected, both edge waves propagate to the left, and simultaneously, there are two bulk waves of a considerably reduced intensity that are swept to the right.

To summarize, we proposed and analyzed a general feedback-based method for realizing topological mechanical metamaterials with arbitrary responses that are not constrained by Newton's laws of motion. As an example, we implemented two topological two-band systems analogous to the quantum Haldane, and the modified Haldane model, in a classical-mechanical metamaterial. The required non-Newtonian complex-valued directional couplings between masses were generated via autonomous real-time control. We demonstrated that the resulting systems have all the properties of the quantum models, and support the expected wave propagation along the metamaterial edges. The method is general, and could be programmed to implement a wide variety of topological models in classical systems, relying both on Newtonian and non-Newtonian dynamics. To stress this point, in the Supplemental Material [47] we designed a pseudospin multipole topological insulator on the same hardware platform, yet with different feedback software. The resulting system mimics the quantum spin Hall effect [29], but without any spinning elements, using out-of-plane d.o.f. alone.

We thank Moshe Goldstein and Daniel Sabsovich for fruitful discussions. This research was supported in part by the Israel Science Foundation Grants No. 968/16 and No. 2096/18, by the Israeli Ministry of Science and Technology Grant No. 3-15671, by the US-Israel Binational Science Foundation Grant No. 2018226, and by the National Science Foundation Grant No. NSF PHY-1748958.

Note added.—We recently became aware of the following related article [48].

*leabeilkin@tauex.tau.ac.il

[1] D. J. Thouless, M. Kohmoto, M. P. Nightingale, and M. den Nijs, Quantized Hall Conductance in a Two-Dimensional Periodic Potential, Phys. Rev. Lett. **49**, 405 (1982).
[2] F. D. M. Haldane, Model for a Quantum Hall Effect without Landau Levels: Condensed-Matter Realization of the "Parity Anomaly", Phys. Rev. Lett. **61**, 2015 (1988).
[3] C. L. Kane and E. J. Mele, Quantum Spin Hall Effect in Graphene, Phys. Rev. Lett. **95**, 226801 (2005).
[4] B. A. Bernevig, T. L. Hughes, and S.-C. Zhang, Quantum spin Hall effect and topological phase transition in HgTe quantum wells, Science **314**, 1757 (2006).
[5] A. B. Khanikaev, R. Fleury, S. H. Mousavi, and A. Alù, Topologically robust sound propagation in an angular-momentum-biased graphene-like resonator lattice, Nat. Commun. **6**, 8260 (2015).
[6] C. He, X. Ni, H. Ge, X.-C. Sun, Y.-B. Chen, M.-H. Lu, X.-P. Liu, and Y.-F. Chen, Acoustic topological insulator and robust one-way sound transport, Nat. Phys. **12**, 1124 (2016).
[7] Z. Zhang, Q. Wei, Y. Cheng, T. Zhang, D. Wu, and X. Liu, Topological Creation of Acoustic Pseudospin Multipoles in a Flow-Free Symmetry-Broken Metamaterial Lattice, Phys. Rev. Lett. **118**, 084303 (2017).
[8] S. Yves, R. Fleury, F. Lemoult, M. Fink, and G. Lerosey, Topological acoustic polaritons: Robust sound manipulation at the subwavelength scale, New J. Phys. **19**, 075003 (2017).
[9] M. Hafezi, S. Mittal, J. Fan, A. Migdall, and J. Taylor, Imaging topological edge states in silicon photonics, Nat. Photonics **7**, 1001 (2013).
[10] W.-J. Chen, S.-J. Jiang, X.-D. Chen, B. Zhu, L. Zhou, J.-W. Dong, and C. T. Chan, Experimental realization of photonic topological insulator in a uniaxial metacrystal waveguide, Nat. Commun. **5**, 5782 (2014).
[11] G. Harari, M. A. Bandres, Y. Lumer, M. C. Rechtsman, Y. D. Chong, M. Khajavikhan, D. N. Christodoulides, and M. Segev, Topological insulator laser: Theory, Science **359**, eaar4003 (2018).
[12] M. A. Bandres, S. Wittek, G. Harari, M. Parto, J. Ren, M. Segev, D. N. Christodoulides, and M. Khajavikhan,

Topological insulator laser: Experiments, Science **359**, eaar4005 (2018).
[13] T. Ozawa, H. M. Price, A. Amo, N. Goldman, M. Hafezi, L. Lu, M. C. Rechtsman, D. Schuster, J. Simon, O. Zilberberg, and I. Carusotto, Topological photonics, Rev. Mod. Phys. **91**, 015006 (2019).
[14] M. C. Rechtsman, J. M. Zeuner, Y. Plotnik, Y. Lumer, D. Podolsky, F. Dreisow, S. Nolte, M. Segev, and A. Szameit, Photonic Floquet topological insulators, Nature (London) **496**, 196 (2013).
[15] G. Salerno, T. Ozawa, H. M. Price, and I. Carusotto, Floquet topological system based on frequency-modulated classical coupled harmonic oscillators, Phys. Rev. B **93**, 085105 (2016).
[16] R. Fleury, A. B. Khanikaev, and A. Alù, Floquet topological insulators for sound, Nat. Commun. **7**, 11744 (2016).
[17] Y.-G. Peng, C.-Z. Qin, D.-G. Zhao, Y.-X. Shen, X.-Y. Xu, M. Bao, H. Jia, and X.-F. Zhu, Experimental demonstration of anomalous Floquet topological insulator for sound, Nat. Commun. **7**, 13368 (2016).
[18] C. H. Lee and R. Thomale, Anatomy of skin modes and topology in non-Hermitian systems, Phys. Rev. B **99**, 201103(R) (2019).
[19] C. Scheibner, W. T. Irvine, and V. Vitelli, Non-Hermitian Band Topology and Skin Modes in Active Elastic Media, Phys. Rev. Lett. **125**, 118001 (2020).
[20] M. I. Rosa and M. Ruzzene, Dynamics and topology of non-Hermitian elastic lattices with non-local feedback control interactions, New J. Phys. **22**, 053004 (2020).
[21] M. Brandenbourger, X. Locsin, E. Lerner, and C. Coulais, Non-reciprocal robotic metamaterials, Nat. Commun. **10**, 4608 (2019).
[22] T. Helbig, T. Hofmann, S. Imhof, M. Abdelghany, T. Kiessling, L. Molenkamp, C. Lee, A. Szameit, M. Greiter, and R. Thomale, Generalized bulk-boundary correspondence in non-Hermitian topolectrical circuits, Nat. Phys. **16**, 747 (2020).
[23] P. Delplace, J. Marston, and A. Venaille, Topological origin of equatorial waves, Science **358**, 1075 (2017).
[24] R. Süsstrunk and S. D. Huber, Observation of phononic helical edge states in a mechanical topological insulator, Science **349**, 47 (2015).
[25] P. Wang, L. Lu, and K. Bertoldi, Topological Phononic Crystals with One-Way Elastic Edge Waves, Phys. Rev. Lett. **115**, 104302 (2015).
[26] L. M. Nash, D. Kleckner, A. Read, V. Vitelli, A. M. Turner, and W. T. Irvine, Topological mechanics of gyroscopic metamaterials, Proc. Natl. Acad. Sci. U.S.A. **112**, 14495 (2015).
[27] S. H. Mousavi, A. B. Khanikaev, and Z. Wang, Topologically protected elastic waves in phononic metamaterials, Nat. Commun. **6**, 8682 (2015).
[28] R. K. Pal and M. Ruzzene, Edge waves in plates with resonators: An elastic analogue of the quantum valley Hall effect, New J. Phys. **19**, 025001 (2017).
[29] R. Chaunsali, C.-W. Chen, and J. Yang, Subwavelength and directional control of flexural waves in zone-folding induced topological plates, Phys. Rev. B **97**, 054307 (2018).
[30] Y. Zhou, P. R. Bandaru, and D. F. Sievenpiper, Quantum-spin-Hall topological insulator in a spring-mass system, New J. Phys. **20**, 123011 (2018).
[31] T.-W. Liu and F. Semperlotti, Design and experimental validation on acoustic valley Hall edge states in reconfigurable phononic elastic waveguides, J. Acoust. Soc. Am. **145**, 1687 (2019).
[32] S. S. Ganti, T.-W. Liu, and F. Semperlotti, Topological edge states in phononic plates with embedded acoustic black holes, J. Sound Vib. **466**, 115060 (2020).
[33] H. Pan, Z. Li, C.-C. Liu, G. Zhu, Z. Qiao, and Y. Yao, Valley-Polarized Quantum Anomalous Hall Effect in Silicene, Phys. Rev. Lett. **112**, 106802 (2014).
[34] A. Souslov, B. C. van Zuiden, D. Bartolo, and V. Vitelli, Topological sound in active-liquid metamaterials, Nat. Phys. **13**, 1091 (2017).
[35] E. Colomés and M. Franz, Antichiral Edge States in a Modified Haldane Nanoribbon, Phys. Rev. Lett. **120**, 086603 (2018).
[36] D. Bhowmick and P. Sengupta, Antichiral edge states in Heisenberg ferromagnet on a honeycomb lattice, Phys. Rev. B **101**, 195133 (2020).
[37] M. Mannaï and S. Haddad, Strain tuned topology in the Haldane and the modified Haldane models, J. Phys. Condens. Matter **32**, 225501 (2020).
[38] S. Mandal, R. Ge, and T. C. H. Liew, Antichiral edge states in an exciton polariton strip, Phys. Rev. B **99**, 115423 (2019).
[39] P. Zhou, G.-G. Liu, Y. Yang, Y.-H. Hu, S. Ma, H. Xue, Q. Wang, L. Deng, and B. Zhang, Observation of photonic antichiral edge states, arXiv:2009.01021.
[40] Y. Chen, G. Hu, and G. Huang, A hybrid elastic metamaterial with negative mass density and tunable bending stiffness, J. Mech. Phys. Solids **105**, 179 (2017).
[41] B.-I. Popa, D. Shinde, A. Konneker, and S. A. Cummer, Active acoustic metamaterials reconfigurable in real time, Phys. Rev. B **91**, 220303(R) (2015).
[42] F. Zangeneh-Nejad and R. Fleury, Active times for acoustic metamaterials, Rev. Phys. **4**, 100031 (2019).
[43] L. Sirota, F. Semperlotti, and A. M. Annaswamy, Tunable and reconfigurable mechanical transmission-line metamaterials via direct active feedback control, Mech. Syst. Signal Process. **123**, 117 (2019).
[44] L. Sirota and A. M. Annaswamy, Active boundary and interior absorbers for one-dimensional wave propagation: Application to transmission-line metamaterials, Automatica **117**, 108855 (2020).
[45] A. Darabi, M. Collet, and M. J. Leamy, Experimental realization of a reconfigurable electroacoustic topological insulator, Proc. Natl. Acad. Sci. U.S.A. **117**, 16138 (2020).
[46] T. Hofmann, T. Helbig, C. H. Lee, M. Greiter, and R. Thomale, Chiral Voltage Propagation and Calibration in a Topolectrical Chern Circuit, Phys. Rev. Lett. **122**, 247702 (2019).
[47] See Supplemental Material at http://link.aps.org/supplemental/10.1103/PhysRevLett.125.256802 for Non-Newtonian mechanical metamaterials using feedback control.
[48] A. Ghatak, M. Brandenbourger, J. van Wezel, and C. Coulais, Observation of non-Hermitian topology and its bulk–edge correspondence in an active mechanical metamaterial, Proc. Natl. Acad. Sci. U.S.A. **117**, 29561 (2020).